DESIGNING FOUNDATIONS ON CLAY TO LIMIT IMMEDIATE MOVEMENTS

M D Bolton MA, MSc, PhD, CEng, MICE

University Lecturer, Cambridge University Engineering Department

H W Sun BEng, MPhil, PhD

Geotechnical Engineer, W S Atkins Consultants Limited

INTRODUCTION

It is straightforward in geotechnical design to estimate the collapse load of a foundation. The calculation methods are well established from the theory of plasticity (Terzaghi, 1943). However, displacements under working conditions are more important in most cases. Simple but accurate deformation calculations are unavailable. Displacement serviceability conditions are often met instead by the adoption of a soil peak strength reduced by a "Factor of Safety" in the plastic collapse calculations. Otherwise, linear elastic solutions (Poulos and Davies, 1974) are employed. However, the selection of an elastic stiffness "constant" for a non-linear soil response has proved to be an intractable problem.

In this paper, a simple deformation mechanism, which directly utilizes the non-linear stress-strain curve of the foundation soil, is proposed for the estimation of immediate settlement under a strip footing on cohesive soil. The results of this simple calculation are compared with the results of non-linear finite element calculations.

SOIL STRESS-STRAIN RELATION

Correct representation of the stress-strain relation of soil is a key factor for deformation analyses in geotechnical engineering. Jardine et al (1986) used a non-linear curve fitted over stress-strain data , in conjunction with the finite element method, to highlight these effects on soil-structure analyses. Figure 1 shows the typical stress-strain response of overconsolidated kaolin clay shearing in undrained plane strain conditions. This response is highly non-linear, and a power law (Equation 1) is an approximate mathematical formulation for it. This power law will be used in the simple deformation calculation presented later in this paper.

$$\frac{c_{mob}}{c_u} = \left(\frac{\gamma}{\gamma_u}\right)^b \qquad (1)$$

c_{mob} is the mobilized shear strength in undrained shearing at shear strain γ. c_u is the undrained shear strength of the clay and γ_u is the shear strain at which the plateau of c_u is first attained. c_u, γ_u and b are the governing factors for a non-linear stress-strain curve. For the response of overconsolidated stiff kaolin in undrained unload reload loops, the exponent b is 0.25. Based on triaxial tests with internal strain measurements on six natural stiff clays in the UK (O'Brien et al, 1991), γ_u in the range 1 to 4.5 % and b in the range 0.3 to 0.65 were obtained.

This power law relationship represents the measurements taken directly from undrained tests on soil elements. In this model, strain increments are linked directly into stress increments, rather than being deduced from a plastic flow rule linked to a yield surface in a typical work-hardening plasticity model. In the simple application, which follows, there will be no operational difference between the two. If plastic strains are measured in the laboratory as stresses traverse a single monotonic stress path under investigation, those strains must be considered axiomatically correct. It does not matter whether they are inserted directly into a simple "power law" soil description, or into some constitutive model of work-hardening plasticity which is coaxed into generating the same strain indirectly. Obviously, the simple "power law" will be much more user-friendly in routine deformation calculations, whilst being unable, without revision,

to deal with more complex stress-path effects.

FINITE ELEMENT CALCULATIONS

A series of finite element analyses was carried out with a modified version of CRISP90 which ran on the Cambridge University IBM3084 computer. The current standard version of CRISP90 is described in detail by Britto and Gunn (1990).

The non-linear soil stress-strain response as defined by Equation 1 was adopted in the analyses. This soil response can be viewed as fully representative of all "plastic" types of calculation conforming to data such as that of Figure 1, and applies to an isotropic soil body with no history of shear strain. Sun (1990) presented an approach in non-linear finite element calculation to consider stiffness anisotropy of an overconsolidated stiff clay foundation.

Table I presents the parameters of the non-linear curves used in this series of finite element analyses.

Figure 2 shows the 105 element finite element mesh. The mesh was intended to model a 4 m wide prototype flexible footing on a 15 m thick stiff cohesive soil. The lateral boundaries of the mesh are 10 m away from the edge of the footing. Footing pressure was applied in small steps up to the maximum value of 250 kN/m^2. This maximum pressure seems high compared with the plastic collapse capacity of 360 kN/m^2 derived from c_u = 70 kN/m^2. However, it is more important in footing design that we are able to generate the load-settlement curve quickly by hand. Then we can select an acceptable settlement value and the associated footing pressure in working conditions.

PLASTIC MECHANISMS

Classical plastic mechanisms were developed and used by mechanical engineers for the analysis of metal machining processes. The material was idealized as rigid plastic as the force required was the most important factor in the process. These mechanisms have been adopted and further developed for geotechnical design, of a strip footing for example (Terzaghi, 1943).

Current geotechnical design has been based on

a reduced strength mobilization in the ground by the introduction of a "Factor of Safety" in the collapse equilibrium equation. However, it has not been possible to relate shear strain (based on the reduced strength mobilization) to ground displacement other than empirically.

The proposed method of deformation calculation for strip footing on cohesive soil consists of two deformation mechanisms: the near-field plastic deformation mechanism and the far-field plastic deformation mechanism.

The new style near-field deformation calculation is developed from classical plasticity methods, following suggestions first made in Cambridge in the 1960s (James et al, 1972). The new method links shear strains to foundation displacements using shear deformation mechanisms compatible with stress equilibrium conditions similar to those found in the classical rigid plastic mechanism.

The far-field deformation mechanism is developed from the theory of undrained cavity expansion (Palmer, 1972). A power law stress-strain idealization of the soil is adopted in the calculations. Based on the equilibrium and displacement-compatibility conditions, estimated far-field ground displacements can be added to the footing settlement predicted by the near-field mechanism. These predictions are then compared with the results of the non-linear finite element calculations.

Block Mechanism

Figure 3 shows a block mechanism for the plastic collapse of a strip footing, in which the soil is treated as rigid plastic. The active and passive triangles slide as rigid blocks on infinitely thin slip planes while the plastic fans suffer additional internal distortion. Through a balance of work and plastic dissipation of energy this mechanism offers an upper bound of $(\pi + 2)\ c_u$ to the bearing capacity of the footing, which is identical to the value given as a lower bound by considering equilibrium using the method of characteristics. This mechanism, however, offers no help in deformation calculation. Shear strain is concentrated in the infinitely thin slip planes. The foundation is modelled as rigid until the instant it

fails completely.

Butterfield and Harkness (1971) considered the stepped mobilization of shear strength in rigid plastic Mohr-Coulomb material under a strip footing. Shear strain is again concentrated in the slip lines; material in-between the slip lines is rigid. Although it was able to calculate the proportional displacement within the plastic deformation zone, this advanced block mechanism was still unable to relate ground displacement to shear strain in the soil.

Near Field Plastic Deformation Mechanism

Figure 4 presents a near-field plastic shear deformation mechanism for the analysis of undrained ground deformation under a strip footing. The outline of this mechanism is similar to the conventional block mechanism (Figure 3) but the displacement within the mechanism is gradual so that the finite shear strains can be derived by differentiation. The area outside the mechanism is considered to be rigid at this stage, and displacements are taken to increase linearly within the near field mechanism, in proportion to the distance from its rigid boundary.

The mean plastic shear strain $\overline{\gamma}$ averaged over the whole near-field deformation mechanism can be derived (Bolton and Sun, 1991).

$$\overline{\gamma} = 3.35 \frac{\delta_N}{B} \tag{2}$$

where δ_N is the near-field settlement of the strip footing of width B (Figure 4).

The equilibrium equation which can then be used is in the standard form of the bearing capacity equation.

$$q = (\pi + 2)\, \overline{c}_{mob} \tag{3}$$

The mean shear strain $\bar{\gamma}$ associated with the mean mobilized shear strength $\bar{c}_{mob}$ for the deformation mechanism can now be read off from the plastic hardening curve (Figure 1) and used in the estimation of near-field footing settlement by Equation 2.

Far-Field Deformation Mechanism

Figure 5 shows the ground displacement adjacent to a strip footing calculated from one of the non-linear finite element analyses. Although the pattern of ground displacement adjacent to the footing is closely modelled, there is extra ground displacement caused by shear strains outside the area of intensive shear modelled by the local shear mechanism. A far-field displacement correction to the settlement under the footing can be calculated from a simple model derived from the theory of undrained plane strain cavity expansion (Palmer, 1972).

In this model, as shown in Figure 6, the ground surface is restricted to horizontal displacement (no ground heave adjacent to the footing) while the semi-circular area immediately under the footing is assumed to be "fluidized".

Two approaches were considered for the estimation of far-field displacement. The first method is based on the shear strain mobilized in the near-field mechanism, and the second one is based on the increase of mean stress in the near-field mechanism.

Assuming no shear strain discontinuity between the near-field and far-field mechanisms at point F of Figure 6, we are able to derive the displacement δ_{F1} due to far-field strains, using displacement compatibility for undrained plane-strain cavity expansion conditions. We know that the shear strain in the active triangle of the near-field mechanism $\gamma_N = 4\ \delta_N / B$. Equation 2 can then be used to show that $\gamma_N = 1.2\ \bar{\gamma}$. Now taking $\gamma_F = 1.2\ \bar{\gamma}$ at a radius $r = B / 2$ in the far-field mechanism, we know that $\gamma_F = 2\ \delta_{F1} / r$ which gives

$$\delta_{F1} = 0.3 \bar{\gamma} B \qquad (4)$$

Otherwise, an estimate of displacement δ_{F2} can be derived from the increase of total mean stress within the active zone of the near-field mechanism. Figure 6 shows the far-field mechanism overlapping the near-field mechanism. The "fluidized" semi-circular area of the cavity expansion model approximately coincides with the active zone of the near-field mechanism. The pressure increase within the cavity is taken to be the increase of mean stress $s = q - \bar{c}_{mob}$ in the active zone. Displacement δ_{F2} at point F due to strain in the far-field can be derived from the equilibrium and compatibility conditions and the power law shear stress-strain relation. It can be shown that

$$\delta_{F2} = \frac{\gamma_u}{4}\left(b\frac{s}{c_u}\right)^{1/b}B \qquad (5)$$

More detailed derivation of Equations 4 and 5 will be presented in Bolton and Sun (1991).

Combined Deformation Mechanism

Settlement under the strip footing can now be estimated by adding the contributions of both near-field and far-field deformation mechanisms. Based on the strain continuity condition, the settlement δ_{T1} predicted by the combined mechanism can be obtained by combining Equations 1, 2, 3 and 4.

$$\frac{\delta_{T1}}{B} = I_1\gamma_u\left(\frac{q}{5.14c_u}\right)^{1/b} \qquad (6)$$

where $I_1 = 0.6$.

Otherwise, combining Equations 1, 2, 3 and 5 leads to a settlement prediction δ_{T2} involving approximate stress continuity.

$$\frac{\delta_{T2}}{B} = I_2\gamma_u\left(\frac{q}{5.14c_u}\right)^{1/b} \qquad (7)$$

where $I_2=[0.125\ \pi\ (4\ b)^{1/b} + 0.3]$

Equations 6 and 7 are identical except that I_1 is not equal to I_2. For power law exponent $b > 0.25$ (Equation 1), δ_T values calculated from I_2 are higher than that from I_1. Figure 7 presents plots of I against exponent b. It shows the results of the non-linear finite element calculations which are normalized using Equations 8 and 9.

$$\frac{\delta_{ave}}{B} = I_{ave}\gamma_u\left(\frac{q}{5.14c_u}\right)^{1/b} \qquad (8)$$

$$\frac{\delta_{max}}{B} = I_{max}\gamma_u\left(\frac{q}{5.14c_u}\right)^{1/b} \qquad (9)$$

where δ_{ave} is the average settlement under the width of the strip load and δ_{max} is the maximum settlement under the centre of the strip load.

It is obvious from Figure 7 that I_{ave} and I_{max} as determined by the non-linear finite element analyses are functions of b. Equation 6 based on shear strain continuity, and Equation 7 based on equilibrium with the mean stress in the active zone of the near field mechanism are also charted in Figure 7. They form lower and upper bounds to the average settlement values of the non-linear finite element analyses, for which $I_{ave} \approx 0.7 + 0.1\ (4\ b)^{1/b}$.

The I_{ave} and I_{max} factors as determined by this series of non-linear finite element analyses as shown in Figure 7 can be applied in routine undrained settlement calculations for strip footings involving a non-linear soil stress-strain relation of the form defined in Equation 1.

WORKED EXAMPLE

A 2 m strip footing is to be founded on the surface of a 10 m thick London Clay overlying very stiff Woolwich Beds, which are assumed to be rigid. A good quality sample of the London Clay tested in an undrained triaxial test with internal strain measurement showed that the stress-strain curve could be represented by the power law:

$$\frac{c_{mob}}{c_u} = \left(\frac{\gamma}{\gamma_u}\right)^b$$

with c_u = 70 kN/m^2, γ_u = 2% and b = 0.5.

A conventional design calculation is performed. An allowable bearing pressure q is given by

$$q = 5.14 \frac{c_u}{FOS}$$

Using FOS = 2.5, q = 140 kN/m^2 is obtained. However, the undrained settlement under this load is still unknown.

We now use Equation 8 and design chart (Figure 7), for b = 0.5

$$\frac{\delta_{ave}}{B} = 0.92 \gamma_u \left(\frac{q}{5.14 c_u} \right)^{1/b}$$

$$\delta_{ave} = 0.006m$$

This shows that 6 mm immediate settlement is to be anticipated under the footing pressure of 140 kN/m^2.

CONCLUSION

Ground deformations are often more localized then those predicted by linear elastic solutions. Undrained plastic deformation mechanisms based on the method of characteristics resembled patterns of undrained ground deformation predictions of non-linear finite element calculations. Cavity expansion models offer simple approaches in the estimation of displacement due to far-field strains involving a non-linear soil stress-strain relation. It leads to the establishment of the semi-empirical I factors and Equations 8 and 9 for the estimation of settlement under a strip footing based on a series of non-linear finite element analyses.

It is now possible to use mobilized soil strength in simple bearing capacity type formulae, to relate soil strain and ground deformation with realistic soil stress-strain curves. The accuracy of the deformation mechanism approach for displacement predictions of non-linear finite element calculations is apparently sufficient to form the basis of a new geotechnical design method.

ACKNOWLEDGEMENTS

The opinions expressed here are the authors' and do not necessarily coincide with those of the Cambridge University and WS Atkins Consultants Ltd.

Wing Sun is grateful for the support of his colleague of WS Atkins Geotechnical Division, particularly Dermod Sweeney, Tony O'Brien and Dr C K Lau in the production of this paper.

REFERENCES

Bolton M D and SUN H W - Plasticity Deformation Mechanisms for the Calculation of Immediately Ground Movements due to Loading on Clays, to be submitted for publication in Géotechnique, (1991)

Britto A M and Gunn M J - CRISP90 User's and Programmer's Guide, Cambridge University Engineering Department, (1990).

Butterfield R and Hardness R M - The Kinematics of Mohr-Coulomb Materials, Stress-Strain Behavior of Soils - Proceedings of the Roscoe Memorial Symposium, Cambridge University, (1971), 220-233.

James R G, Smith I A A and Brandsby P L - The Prediction of Stress and Deformations in a Sand Mass Adjacent to a Retaining Wall, Proceedings of the 5th European Conference on Soil Mechanics and Foundation Engineering, Madrid, (1972) Vol1, 39-46.

Jardine R J, Potts D M, Fourie A B and Burland J B - Studies of the Influence of Non-Linear Stress-Strain Characteristics in Soil-Structure Interaction, Géotechnique, 36, (1986), 377-396.

O'Brien A S, Forbes-King C J, Gildea P A and Sharp P - The Assessment of In Situ Stress and Stiffness at Seven Overconsolidated Clay and Weak Rock Sites, Submitted for publication in Ground Engineering, (1991).

Palmer A C - Undrained Plane-Strain Expansion of a Cylindrical Cavity in Clay: A Simple Interpretation of the Pressuremeter Test, Géotechnique, 22 (3), (1972), 451-457.

Poulus H G and Davies E H - Elastic Solutions for Soil and Rock Mechanics, John Wiley & Son, (1974).

Sun H W - Ground Deformation Mechanisms for Soil-Structure Interaction, PhD Dissertation, Cambridge University, (1990).

Terzaghi K - Theoretical Soil Mechanics, John Wiley & Son, (1943).

TABLE I Power law stress-strain parameters used in finite element analyses

Finite element analyses	c_u (kN/m^2)	γ_u	b
STFG 1	70	6.0 %	0.25 *
STFG 2	70	1.5 %	0.50
STFG 3	70	1.5 %	0.35
STFG 4	70	1.5 %	0.65
STFG 5	70	3.0 %	0.35
STFG 6	70	3.0 %	0.65

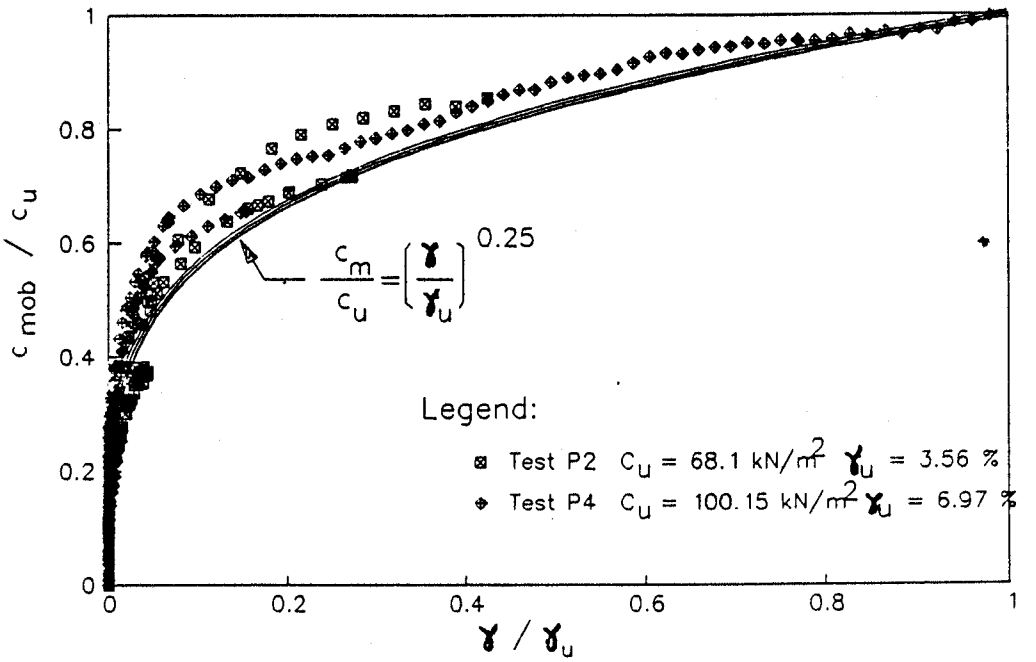

FIGURE 1 Typical response of kaolin following load reversal

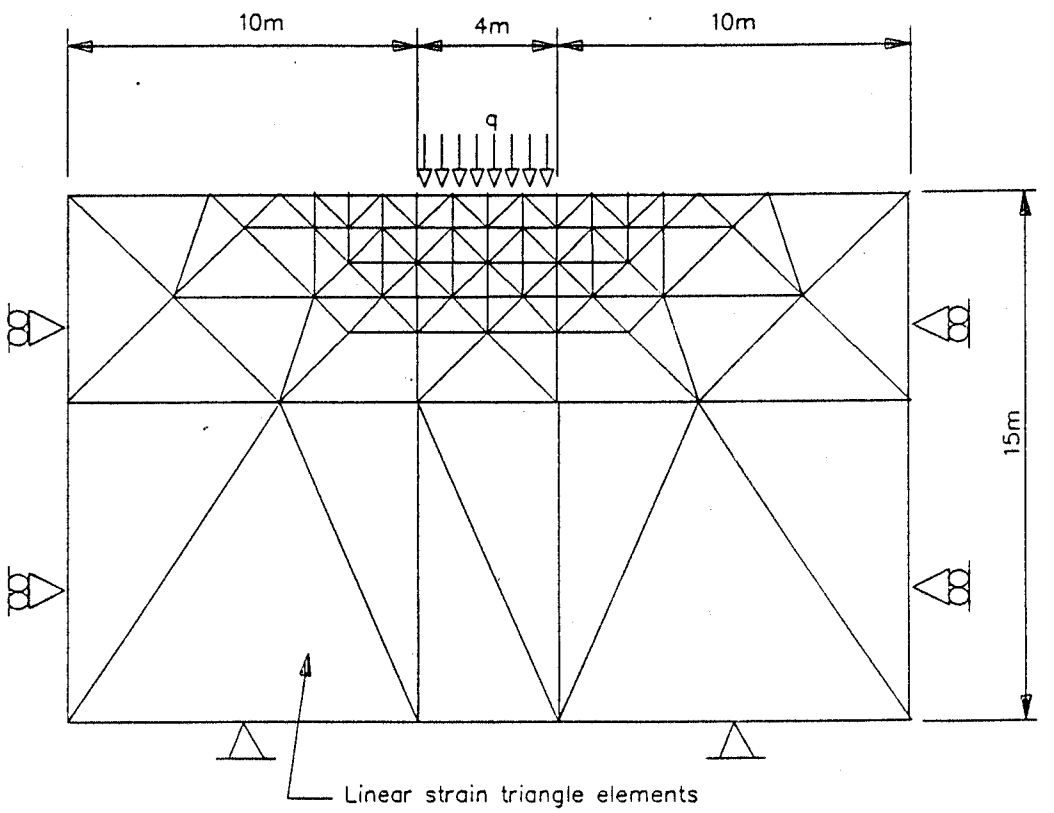

FIGURE 2 General layout of finite element mesh – strip footing

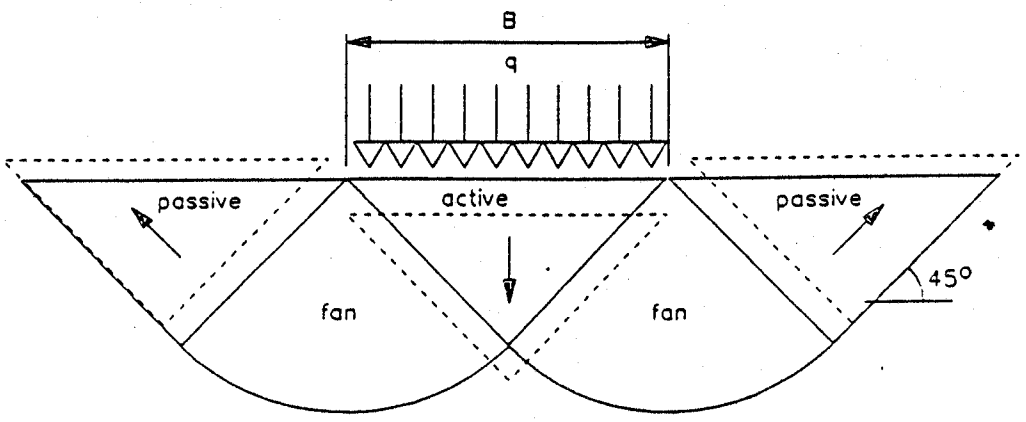

FIGURE 3 Conventional plastic block mechanism – strip footing

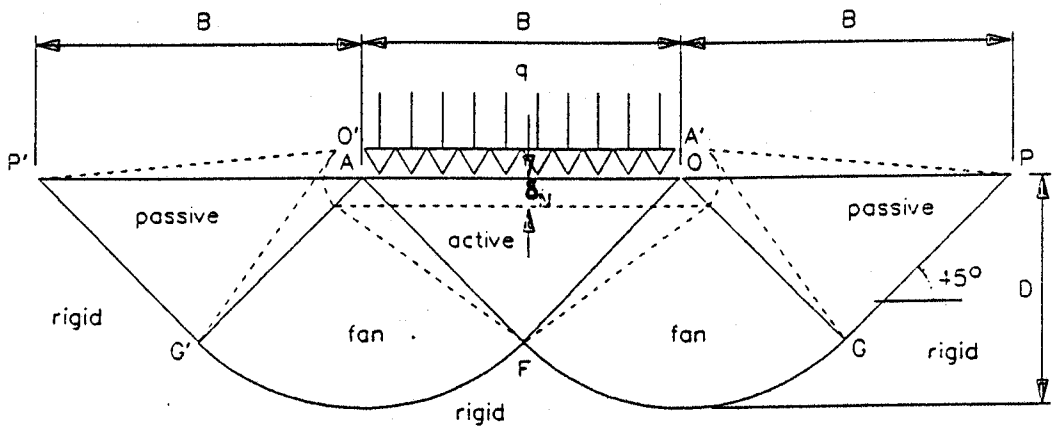

FIGURE 4 Near–field plastic deformation mechanism – strip footing

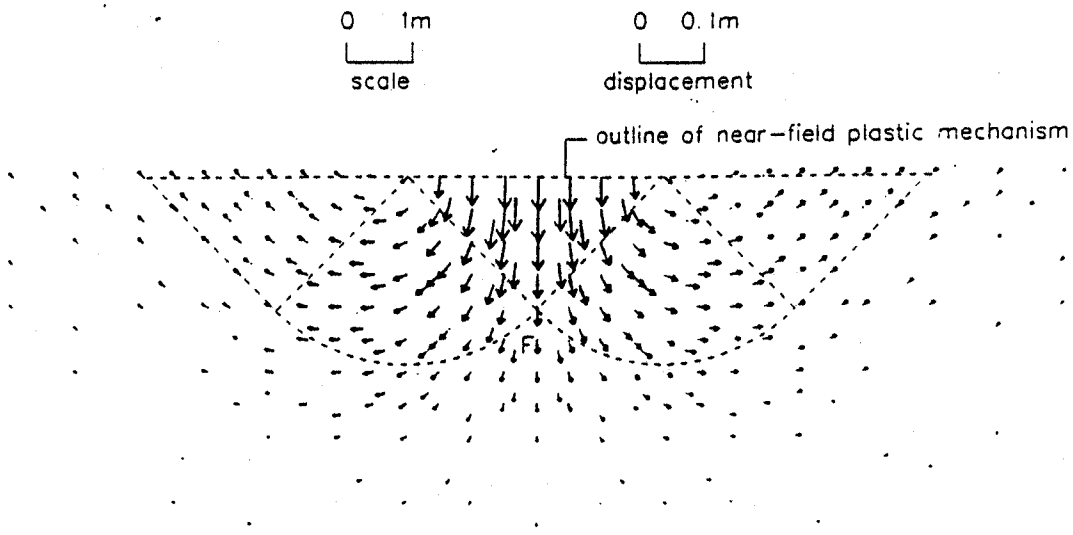

FIGURE 5 Ground displacement under strip footing predicted by finite element calculations

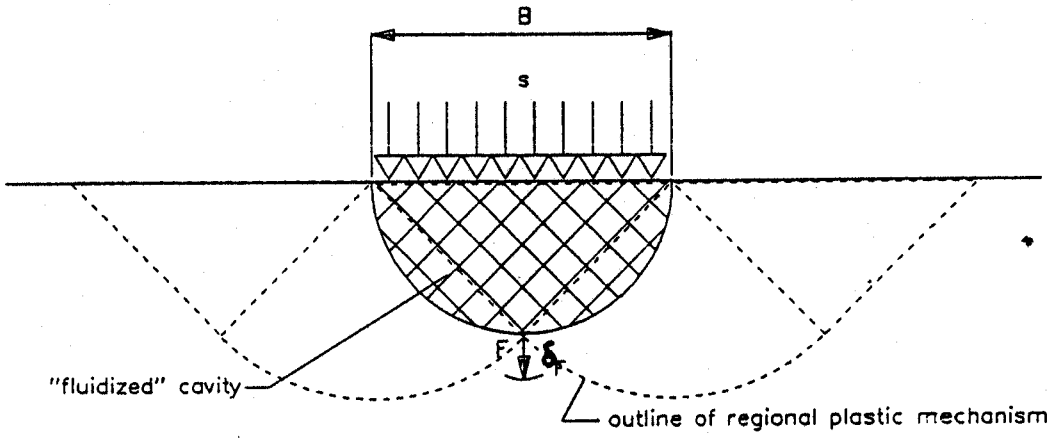

FIGURE 6 Far–field cavity expansion mechanism – strip footing

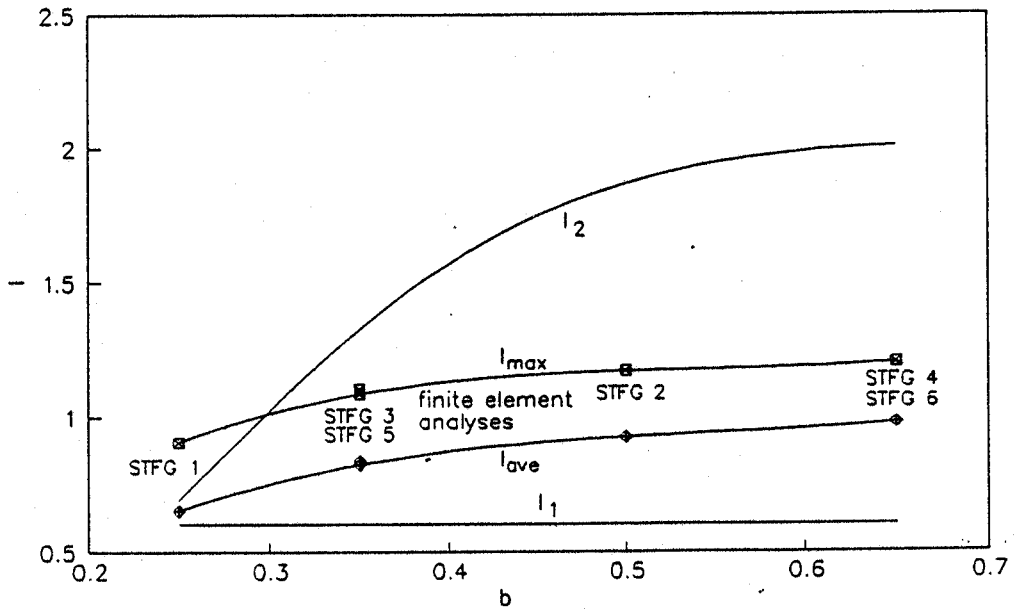

FIGURE 7 I factor vs exponent b – strip footing